Paper No.200

ESTIMATION OF FUTURE DISCHARGES & IMPACT OF CLIMATE CHANGE ON THE HYDROPOWER GENERATION OF NALTAR IV HPP PAKISTAN – 198 MW

Engr. Syed Hammad Ali

ESTIMATION OF FUTURE DISCHARGES & IMPACT OF CLIMATE CHANGE ON THE HYDROPOWER GENERATION OF NALTAR IV HPP PAKISTAN

By

Syed Hammad Ali[1]

Abstract

Water stored in the form of snow and glaciers in the High Mountain Asia (HMA) region regulates the water supply, and resultant water-based economies, that support the livelihoods of millions of people. Trends in the seasonal and long-term melting of snow and glaciers, governed by initial ice reserves, meteorological factors and geographic features, vary across sub-basins in the HMA region. We examined the impacts of climate-led changes in river flow in Hunza basin Karakoram Pakistan. We used an integrated assessment framework (a suite of climate models, snow/glacier-hydrology, and hydropower model) to estimate the changes in discharges and hydropower generation from Naltar hydropower plant on Hunza River fed by snow & glacier melt. We compared the differences in estimated river flow over historic and future time using the water balance model in sixteen scenarios (eight climate models and two emissions scenarios) for river upstream of hydropower plant in Hunza basin. Using the hydropower model we estimated the changes in hydropower generation at the Naltar IV hydropower plant, with an 18 MW capacity, located in Hunza, Karakoram. When compared to the baselines, the estimated impact of climate change and temporal variability were found higher for the Naltar IV plant. Our sensitivity analysis shows that hydropower plants with water storage facilities help reduce the impact of changes, but the estimated impacts are higher for the higher capacity plants. This study provides an example of the impacts of climate change on hydropower generation located in river fed by varying amounts of snow and glacier melt at different decades in this century. This type of integrated assessment of climate change impact will support the scientific understanding of hydrologic flow and its impacts on a hydropower generation under various climate scenarios, as well as generate information about water resource management in a changing climate.

Keywords: remote sensing, hydrology, glaciers, climate change, hydropower, Karakoram anomaly and Himalaya

GCMs

Global Circulation Model (GCM) is a model that simulates general circulation of planetary atmosphere or oceans. The term general circulation is used to indicate large-scale atmospheric or oceanic motions with its persistent as well as transient features on various scales.

[1] Glacier Monitoring Research Centre (GMRC), Pakistan Water and Power Development Authority, Lahore, Pakistan (WAPDA).

WBM

Water balance models (WBM) describe computational aspects of water movement through the water cycle, thus can indeed be considered as a subgroup of hydrological models.

PyGEM

The Python Glacier Evolution Model (PyGEM) is an open-source large-scale glacier evolution model that has been used to project the response of glaciers to climate change at regional and global scales.

Introduction

The hydrology of the HMA region is influenced by the quantity of snowfall and rainfall, the characteristics of the glaciers, the atmospheric temperature in the melt season, and the share of snow & glacier melt in river flows. The extent of westerly and monsoon influence varies with the location of a given sub-basin in the region, but the melting of snow & glaciers differ from sub-basin to sub-basin depending upon such factors as the quantity, location and orientation of snowpack, solar radiation, rainfall, etc. Governments in this region have been encouraging the development of relatively low-cost electricity production from hydropower plants to meet the increasing demand for electricity in the region.

Information about projected changes in river flow, seasonally and over the century, is important for infrastructure development and planning downstream, including critical hydropower and irrigation infrastructure. Climatic drivers and their influence on the hydrology in the Karakoram are different from those in the Central Himalaya region. Figure-1 shows the locations of the study area in HMA.

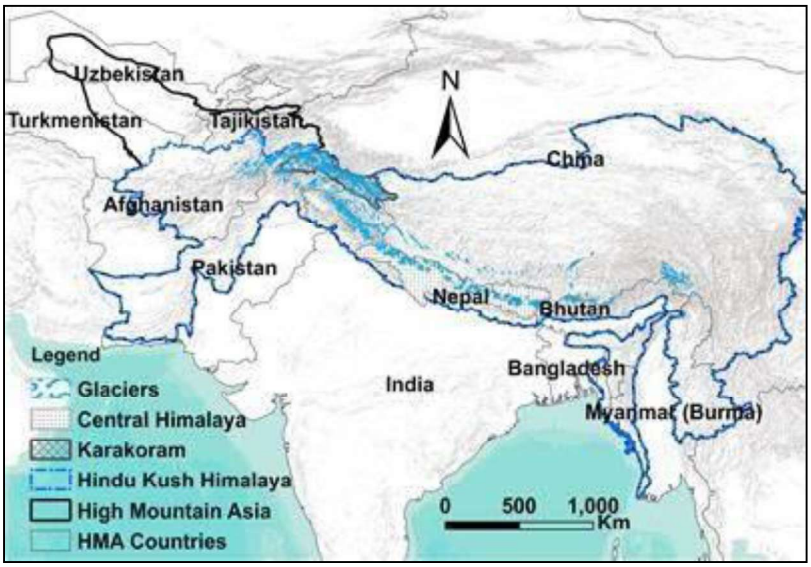


Figure-1: High Mountain Asia, HKKH Karakoram region is the northernmost Pakistan, covered by the glaciers

Fowler and Archer (2006) and Khattak et al. (2011) observed trends of increasing precipitation as well as rising winter mean and maximum temperature (including at high elevations) in the Karakoram region. In the HMA region, the snow cover peaks in winter, but in the Karakoram region of the Upper Indus basin the maximum snow cover occurs in the spring, and a negative winter snow cover trend was observed (Immerzeel et al., 2009). In the Karakoram region, summer precipitation is increasing, but glacier and snowmelt contributions to river flow during the summer season are decreasing.

Glaciers cover 12,500 km^2 of the Karakoram distributed across four sub-basins (Bajracharya et al., 2014). Kraaijenbrink et al. (2017) estimated that by 2099, 64 ± 7% of the ice mass stored in HMA glaciers will remain with a global temperature increase of 1.5°C. Glacier mass loss in Karakoram (ranges from 0.18 to 0.11 m w.e. yr^{-1}) (Lutz, 2016; Brun et al., 2017; Shean et al., 2020). Glaciers in the Karakoram exhibit characteristics of both the "summer accumulation" due to the summer monsoon and the "winter accumulation" due to the winter westerly disturbances (Kapnick et al., 2014; Bashir et al., 2017). The stable or positive rate of glacier mass change in the Karakoram has been associated with trends of increased snow accumulation and attributed to stronger winter westerly disturbances (Forsythe et al., 2017; Smith and Bookhagen, 2018). As a result, the rate of glacier mass change in the Karakoram is neutral or positive. The seasonal changes in river flow pose a threat to downstream economic activities, such as hydropower generation and crop irrigation in the region, because the water demand for hydropower generation and crop irrigation is highest in the spring season.

Pakistan is investing in hydropower development to meet the growing demand for electricity. Pakistan's energy security is considered to be at risk due to the large share of imported fossil fuel in its energy mix (Rehman et al., 2019). Primarily due to supply problems, in 2013 Pakistan typically shed load (cut electricity supply to consumers) up to 8h per day in urban areas and 16–18h in rural areas (Khokhar et al., 2015). To achieve energy security, stability, and reliability goals, the government of Pakistan has promoted renewable development in the energy mix (Kessides, 2013). In 2015, 438MW of hydropower projects were added to the national grid, raising the share of hydropower electricity to 30.4% of the total electricity production in Pakistan (Ministry of Finance, 2013; Ahmed and Suphachalasai, 2014). By 2030, with the completion of 24 hydropower projects, Pakistan is expected to have a total capacity of 42 GW (Water Power Development Authority Report [WAPDA], 2013). The Gilgit-Baltistan (GB) region of the Karakoram is estimated to have a hydropower potential of 19,696 MW (Abbasi et al., 2017). Currently, 126 hydropower plants are operating in the region with an installed capacity of 132 MW. According to the WAPDA GB government, in 2016 the region faced a capacity shortfall of 52MW in the summer and 173MW in the winter. WAPDA is working on mega-hydropower projects with a total capacity of 18,720MW, and 27 of the hydropower projects with a total capacity of 248MW are in Gilgit-Baltistan region (Abbasi et al., 2017).

Earlier studies have focused on climate change impacts on glaciers in larger drainage basins such as the Indus, Ganga, and Brahmaputra basins; however, water resource management decisions take place at a smaller sub-basin scale. Glaciers melt is estimated to contribute 26% of total runoff in Indus basin (Immerzeel and Bierkens, 2012).

A few studies, including Alford and Armstrong (2010), Pradhananga et al. (2014), and Tahir et al. (2015) have looked at hydrological impacts on smaller sub-basins. Tahir et al. (2011) found that (a) 1% increase in snow cover area in Hunza under constant temperature will increase summer discharge by 0.7%, (b) an increase in 1°C mean temperature (keeping precipitation and snow cover constant) is expected to increase summer discharge by 33%, and (c) a 20% increase in snow cover in combination with a 2–4°C rise in mean temperature is expected to increase future stream flows by 100%.

In order to quantify the size and extent of the impacts of river flow changes on hydropower generation of Naltar-II HPP, we generated information on hydrologic flow under various climate change scenarios and estimate the hydropower generation. Specifically, we used sixteen general circulation models (GCM)/RCP combinations to explore a range of possible futures in the Hunza basin. We estimated the hydrologic flow under these climate scenarios using the University of New Hampshire Water Balance Model (WBM). We quantified the impacts on seasonal river flow, with a focus on hydroelectricity generation by using an integrated assessment approach (IAA) developed by Mishra et al. 2018.

Study Area

For this study we select the westerly dominated snow-and glacier-fed Hunza sub-basin of the Karakoram region. The Hunza sub-basin with a surface area of 13,733 km^2 is located in the upper Indus River, with altitudes ranging from 1,415 m to 7,809 m a.s.l. (Figure-2). Sixty-four percent of the sub-basin is at or above an altitude of 4,300 m, 25% of the area is between 3,301 and 4,300 m, and the rest is below 3,300 m. The estimated glacier-covered area in the Hunza is 3,840 km^2 (RGI Consortium, 2017), which is the second highest area under ice and snow among the eight sub-basins of the upper Indus (Bajracharya and Shrestha, 2011). There are several small hydropower plants are operational and large hydropower plants are under construction. The impacts of climate change on river flow in Hunza is assessed using comparative methods that measure the relative difference of river channel flow and hydropower production of Naltar IV hydropower plant using WBM output that is driven by climate model projections.

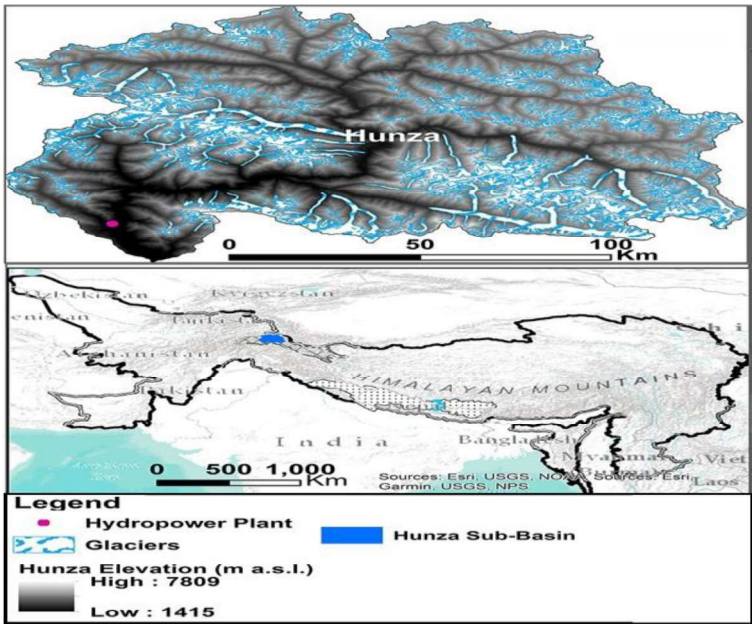


Figure-2: Study Area in HMA Region: Hunza in Karakoram Showing elevation and glaciers and Naltar-IV HPP

Naltar IV has a small reservoir that holds enough water to generate electricity at full capacity for approximately 2h. To a limited extent, the plant can shape hourly water releases during the day such that production is highest during peak load hours. Characteristics of the Naltar power plant are provided in Table-1.

Sr. No.	Characteristics	Naltar IV
1	Commission Date	2007
2	Hydraulic Head	419m
3	Turbine Type	Pelton
4	Capacity	18MW
5	Units (capacity/unit)	3(6 MW)
6	Max Output	18MW
7	Water to Conversion factor	3.53 MW cms-1
8	Diversion Structure Efficiency	100%
9	Outage rate	12.5%

Table-1: Characteristics of Naltar IV HPP

Data & Method

Based on the IAA developed by Mishra et al. (2018), we coupled the principles of climate science, cryosphere sciences, hydrology, and hydropower engineering to analyze impacts of climate change in the Hunza River basin, as illustrated in Figure-3.

Water Balance Model

The University of New Hampshire WBM is a process-based, spatially distributed, gridded model incorporating the major elements of the hydrological cycle. Full model details can be found in for the strong vertical temperature gradients in this region. The model was run for all GCM in all historical and RCP combinations, at daily time steps, at a spatial granularity of 0.8 x 0.8 km grid cells for the entirety of the Hunza basin. Daily river flow was output from the model, and these fields were sampled at the hydropower station location.

WBM Configuration

A digital river network representing surface flow direction clipped from the HydroSHEDS 30 arc-second (approximately0.8 km at these latitudes) resolution dataset for Asia (Lehner and Grill, 2013) downloaded from the USGS HydroSHEDS web site (HydroSHEDS, 2019). This network resolution allowed for a sufficient allocation of land features to represent all relevant hydrological processes in the catchment area of the studied site. No water diversions for irrigation or other human demands (such as domestic, industrial, livestock) have been accounted for, due to limited agricultural hydro-infrastructure development in this high mountainous region. Because climate input variables from the CMIP5 collection are limited, evapotranspiration was simulated using the Hamon method (Hamon, 1961). We use Hamon because of its simplicity and because it has the smallest bias over a range of climate zones (Federer et al., 1996).

Deep ground water aquifers have not been included in the WBM model setup for this study because information and input data layers for Hunza basin are not available.

The elevation grid for the WBM run-time climate downscaling is based on 30 m resolution ASTER DEM v.2 dataset (Tachikawa et al., 2011). A temperature lapse rate of 6.4 km^{1} (Rennick, 1977) is applied at a sub-grid cell resolution to represent elevation gradients within the high-resolution grid cell. This sub-grid cell elevation correction is essential for representing snow accumulation and melt in high elevation gradient regions. All other land cover, soil properties, and basic input layers required to run WBM were taken from Global 30 and 6 arc-minute resolution datasets used in previous global hydrological studies (Vörösmarty et al., 2000; Lammers et al., 2001; Wisser et al., 2010; Liu et al., 2017).

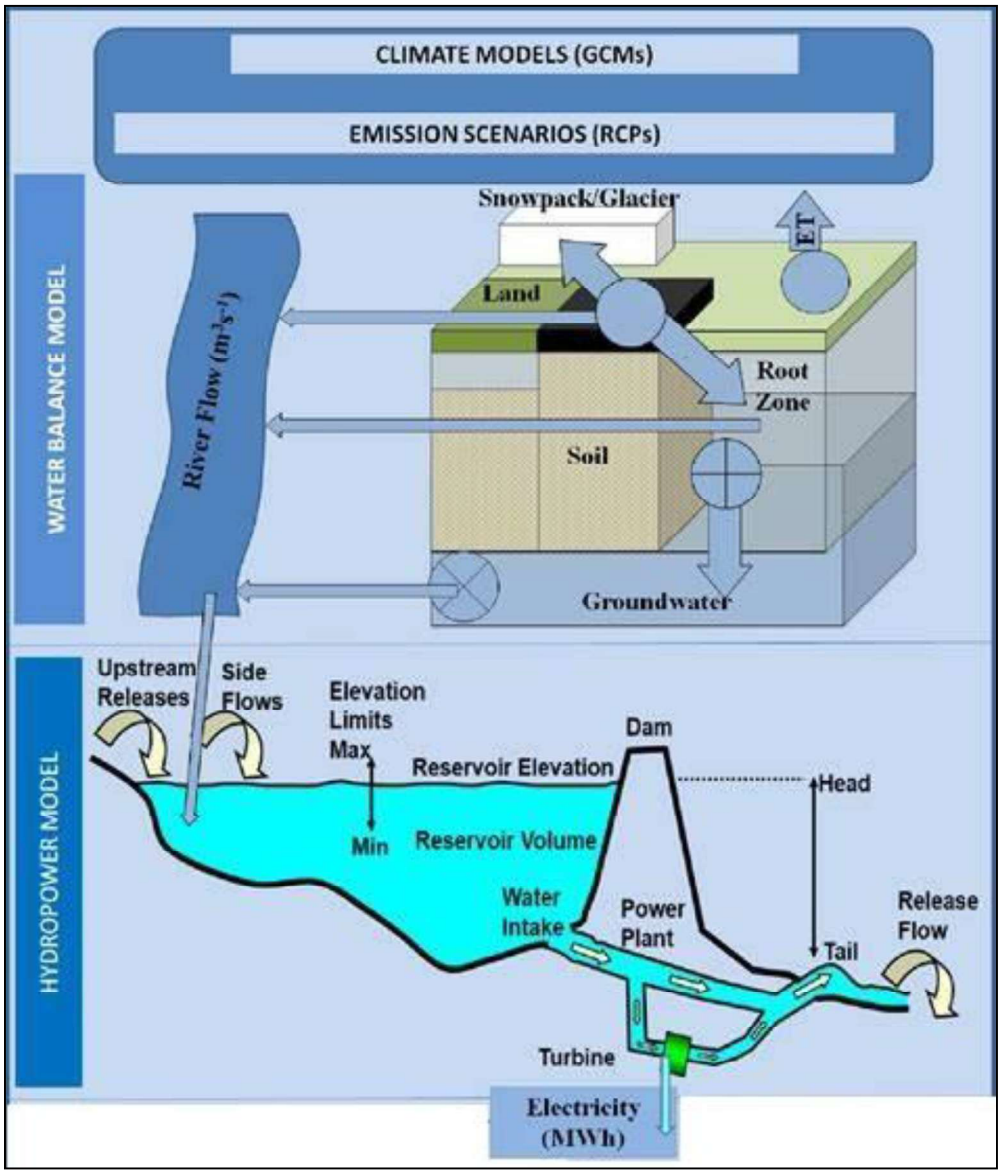


Figure-3: Major Components of the coupled water balance model and hydropower system model

Climate Drivers

Monthly temperature and precipitation are used to drive WBM simulations. The ERA-Interim climate reanalysis dataset (Dee et al., 2011) is used for historical simulations, and CMIP5 GCMs are used for future simulations (Table-2). The spatial resolution of both ERA-Interim and CMIP5 climate drivers are too coarse for this study's domain, due to the steep elevation gradients. To address this issue, two spatial downscaling steps were applied to increase the resolution. First, a

bilinear interpolation was applied to both the temperature and precipitation fields, resulting in a higher-resolution grid scale matching WBM's river network resolution. Second, due to the high elevation gradients in the study domain, an elevation based correction was applied to temperature at the high resolution grid scale. A lapse rate of 6.4 C km^{-1} (Rennick, 1977) was applied based on the elevation difference between the high-resolution river network and the lower-resolution geopotential layer of the climate driver, resulting in elevation based temperature variation at sub-climate driver resolution. In addition to downscaling, we also applied the delta change bias correction method to the GCM climate drivers for future simulations by applying, on a pixel level, the monthly climatology difference between the ERA-Interim and corresponding GCM fields. While WBM represents monthly river flows, it makes use of sub-monthly variability in precipitation. For precipitation, the delta change was applied to a constant daily variability over each month, using year 2001 values, which represents the fewest precipitation extremes (Fekete et al., 2004). Temporal downscaling of temperature does not have a significant effect on the monthly model output used for all analyses in this paper, so a constant monthly temperature was used by WBM to project future water flow rates. Spatial variability, through snowpack formation and melt, is important, and this is discussed in section "Water Balance Model (WBM)."

*For all GCMs, the commonly used "r1i1p1" ensemble was selected. ** These two models bracket the ranges of precipitation represented by the suite of GCMs used in this study and are selected for detailed graphics.

Sr. No.	GCM*	RCP	Variables	(X,Y) in Arc°	
Historical, time series range from October 1999 to September 2017					
	ERA-Interim		12m pr	0.5	0.5
Future, time series range from January 2000 to December 2099					
1	CCSM4	4.5 8.5	Air temperature	1.25	0.94
2	**GFDL-CM3****		(tes),	1.0	1.0
3	GFDL-ESM2M		Precipitation	1.0	1.0
4	GISS-E2-R		Flux(pr)	2.5	2.0
5	**IPSL-CM5A-LR****			3.75	1.9
6	MIROC5			1.4	1.4
7	MRI-CGCM3			1.125	1.12
8	NorESM1-M			2.5	1.9

Table-2: Historical and Future climate CIMP-5 datasets used in WBM simulations

Integrated Glacier Runoff

WBM used output data from the Python Glacier Evolution Model (PyGEM) developed at the University of Alaska at Fairbanks (Rounce et al., 2020; in press). PyGEM estimated the mass balance of every glacier using 10 m elevation bins and a monthly time step. The model was forced with air temperature and precipitation data from the same climate drivers as WBM (Table-2), and computed glacier melt using a degree-day model, accumulation based on a temperature threshold, and refreezing based on mean annual air temperature. Glacier retreat/advance was modeled using mass redistribution curves from curves from Huss and Hock (2015). The model provided glacier runoff, glacier volume, glacier area and other point data variables in the study basins for each glacier in the RGI Version 6.0 database (RGI Consortium, 2017). PyGEM output was rasterized for the study area using the same spatial grid as the river network. Given the monthly temporal resolution of the PyGEM output, no daily temporal downscaling was applied. For each 1 × 1 km grid cell in WBM, glacier outflow was summed and provided as an input to the river system. Precipitation from the GCMs proportional to the glacier area was removed from WBM input precipitation fields to avoid double counting precipitation over the glaciers, because the glacier runoff produced by PyGEM accounts for precipitation, snow accumulation and melt, glacier melt, and refreezing. Hence, all PyGEM outputs (including the water entering the glaciated area as precipitation) are passed to WBM as an input.

River Network and Topography

Digital river networks were used to establish horizontal connectivity of the land surface within drainage basin. Elevation for the snow bands was derived from the 30 m ASTER GDEM v.2 dataset (Tachikawa et al., 2011). Soil properties required to simulate runoff generation in WBM were from the Harmonized World Soil Database v1.2 (Fischer et al., 2008). Data used for calibration and validation included hydrologic flow observation obtained from power plant and stream gauges located at Naltar river basins, from PWD, Pakistan.

The WBM model output provides local runoff, stream flow (river discharge), and primary water source components (fractions) in surface flows and storage. The latter allows tracking of the glacier melt, snowmelt, and rainwater components downstream from the originating runoff grid cells. The component tracking is critical in understanding the stream flow changes over the century in the regions with substantial presence of cryospheric processes, e.g., glacier and snow dynamics.

Hydropower Systems Model (HSM)

To gain a better understanding of the potential impacts of future climates on hydropower operations in the Hunza basin, the hydropower systems model (HSM) was used to estimate daily energy production, in megawatt hours (MWh), between January 1, 2020, and December 31, 2099, inclusive. More specifically, we modeled and analyzed the Naltar-IV hydropower plant located in Hunza basin. Both models take into account power plant capacity and generator unit availability, the

efficiency of converting flowing water to electricity and other plant- specific characteristics presented in Table 1. The WBM model water discharge results are a key HSM driver/predictor of daily hydropower production for power plant. In addition, we modeled water-diversion structures and the routing of water through power plant turbines and flows that circumvent the power plant (non-power water flows). Using historical power plant inflows and generation data, the water-to-power conversion factor used for this study was set to 0.32 MW per cubic-meter per second (MW cms^{-1}). We computed the maximum turbine flow rate using this power conversion factor and the capacity of the plant. Daily generation levels were simulated for each plant for 16 GCM/RCP combinations. For computational efficiency, we used a simulation model that projects daily unit-level generation levels under a large number of unit on/off states, in which a randomly drawn "off " state represents a unit outage. On and off states were estimated for each day of the 2020–2099 time periods using a random number generator. Various random trials were modeled, all of which had similar results. For consistency among RCP 4.5 and RCP 8.5 HSM runs, all model runs used the same set of random draws. The selected outage set was nearly identical to the target outage.

The representation of Naltar in the HSM is based primarily on information supplied by the PWD and turbine efficiency surface for Pelton turbines. Modeled power generation at Naltar uses WBM daily simulated water discharges and an adjusted power conversion efficiency surface. Naltar turbines typically generate more than 10 times the amount of electricity per volume of turbine water release. The water diversion structure that is located upstream of Naltar is capable of redirecting virtually all of the Naltar River to the channel that connects the river to the reservoir.

The HSM also accounts for plant outages and idle hours. These include outages for scheduled maintenance that occur during the months of February, June, September, and December. Based on historical outage levels, HSM assumed that each unit would be available 90% of the time. Historically, each unit is on average "idle" approximately 90 min per day.

RESULTS

Analysis of WBM Stream flow for 21st Century Projections

We present variability and trends of projected annual, decadal, mid-century and end of century hydrological regimes in the Hunza basin (see Table-3 for Mann-Kendall test and Sen's slope analysis results). In most GCM/RCP combinations, the summer discharge initially tends to increase by about 10% at the mid-century, and then experience a sharper decline by about 50% toward the end of the 21st century (Figure-4).

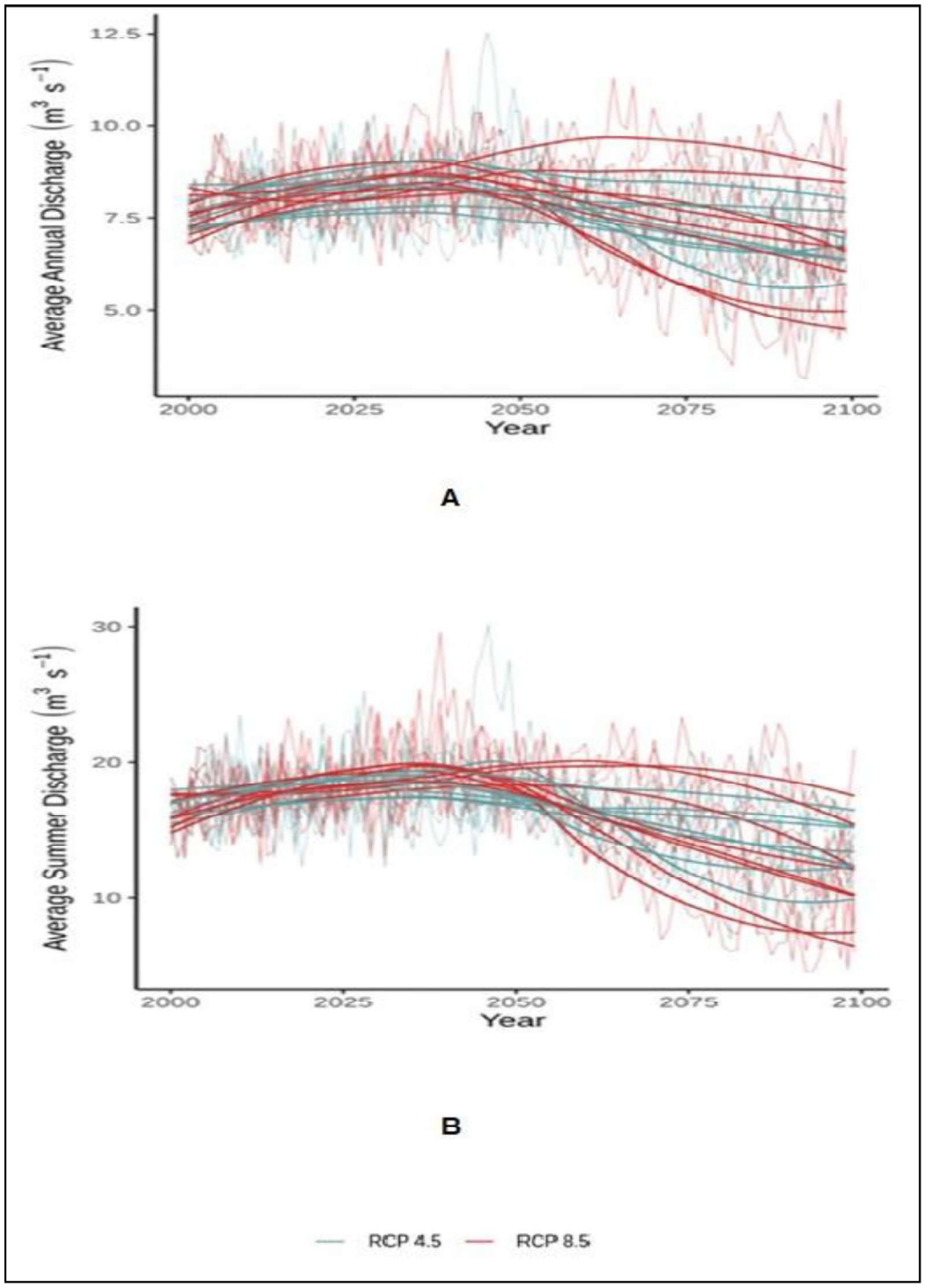


Figure-4: A. Average Annual Discharge B. Average Summer (JJA) Discharge

Average Annual Discharge								
RCP 4.5								
	CCSM4	GFDL-CM3	GFDL-ESM2M	GISS-E2-R	IPSL-CM5A-LR	MIROC5	MRI-CGCM3	NorESM1-M
Tau	-0.153	-0.463	-0.277	-0.475	-0.444	-0.504	-0.157	-0.503
p	0.024	0.000	0.000	0.000	0.000	0.000	0.021	0.000
Sen's slope	-0.007	-0.04	-0.021	-0.03	-0.023	-0.044	-0.007	-0.027
RCP 8.5								
	CCSM4	GFDL-CM3	GFDL-ESM2M	GISS-E2-R	IPSL-CM5A-LR	MIROC5	MRI-CGCM3	NorESM1-M
Tau	-0.256	-0.531	-0.249	-0.375	-0.488	-0.474	0.249	-0.432
p	0.000	0.000	0.000	0.000	0.000	0.000	0.000	0.000
Sen's slope	-0.016	-0.052	-0.017	-0.025	-0.04	-0.043	0.014	-0.025
Average Summer (JJA) Discharge								
RCP 4.5								
	CCSM4	GFDL-CM3	GFDL-ESM2M	GISS-E2-R	IPSL-CM5A-LR	MIROC5	MRI-CGCM3	NorESM1-M
Tau	-0.07	-0.183	-0.242	-0.704	-0.506	-0.14	-0.28	-0.147
p	0.301	0.007	0.000	0.000	0.000	0.039	0.000	0.031
Sen's slope	-0.347	-0.736	-1.589	-1.222	-1.226	-0.619	-1.921	-0.666
RCP 8.5								
	CCSM4	GFDL-CM3	GFDL-ESM2M	GISS-E2-R	IPSL-CM5A-LR	MIROC5	MRI-CGCM3	NorESM1-M
Tau	-0.36	-0.579	-0.343	-0.565	-0.579	-0.529	-0.268	-0.571
p	0.000	0.000	0.000	0.000	0.000	0.000	0.000	0.000
Sen's slope	-0.038	-0.148	-0.068	-0.1	-0.083	-0.129	-0.03	-0.086

Table-3: Mann-Kendall and Sen's Slope results

Annual changes are primarily driven by changes in spring and early summer flows (April to June). These increase significantly (over 90.4) by the middle of the 21st century (Tables 4), due to temperature- enhanced snow and glacier melt, until the time of peak-water (Figure-S5), which occurs in 2050–2080.

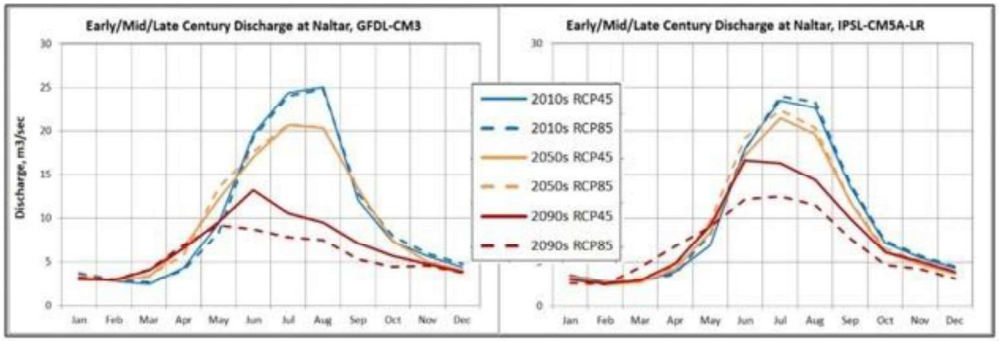


Figure-S5: Average inter-annual changes of discharge for 2010/2050/2090 decades by select GCM/RCPs projections

Toward the end of the century, the model predicts a moderate decline in stream flow (3.6%) during the summer and fall seasons (July to August), compared to contemporary hydrology represented by WBM simulations for ERA-Interim (2000–2017) climate drivers (Tables 4).

GCM	RCP	Decade	January	February	March	April	May	June	July	August	September	October	November	December
CCSM4	RCP45	2050s	49.3	49.4	55.0	43.3	64.4	81.2	48.4	38.9	71.0	61.6	55.7	53.2
		2090s	25.3	25.5	35.2	28.3	51.1	78.6	29.5	12.5	39.2	30.1	23.2	22.7
	RCP85	2050s	47.6	47.9	58.4	78.0	68.8	76.6	53.4	42.5	62.2	56.1	50.8	47.9
		2090s	12.4	22.7	51.8	68.4	105.1	71.6	19.7	1.3	24.2	25.6	18.2	16.1
GFDL-CM3	RCP45	2050s	22.0	28.0	84.1	181.1	150.1	60.1	23.1	19.6	54.3	30.0	13.3	15.2
		2090s	8.2	33.1	121.6	187.6	101.6	24.0	−37.4	−44.1	−17.6	−0.3	7.6	8.7
	RCP85	2050s	13.9	26.8	88.6	150.9	184.2	65.8	23.6	19.9	63.1	30.9	11.1	14.8
		2090s	15.8	36.4	126.1	203.0	93.4	−18.1	−53.6	−55.9	−38.7	−21.5	3.0	7.3
GFDL-ESM2M	RCP45	2050s	78.4	78.5	75.8	15.2	29.5	35.5	52.6	58.8	106.8	85.3	77.7	77.9
		2090s	73.1	73.2	69.6	25.6	67.9	53.7	30.2	25.4	66.4	74.7	68.4	68.6
	RCP85	2050s	84.2	84.3	80.4	21.9	48.2	52.4	59.8	64.1	113.5	94.1	86.3	86.6
		2090s	53.9	54.0	54.2	46.2	135.4	85.5	21.7	8.1	47.8	61.6	52.9	52.7
GISS-E2-R	RCP45	2050s	7.5	9.6	41.4	87.1	93.8	62.0	23.6	20.9	43.7	19.1	14.4	13.0
		2090s	18.8	20.7	47.2	103.7	78.6	23.9	−5.9	−3.6	15.4	25.7	21.9	22.2
	RCP85	2050s	30.6	33.2	56.5	118.4	130.1	67.0	28.0	26.0	55.6	36.0	31.6	29.7
		2090s	35.1	41.1	88.7	148.6	126.8	25.6	−15.3	−8.3	22.5	26.2	35.9	30.5
IPSL-CM5A-LR	RCP45	2050s	7.9	8.4	48.1	95.2	76.9	61.6	27.9	15.5	37.3	7.9	7.2	5
		2090s	9.7	13.4	63.5	113.5	93	56.3	−2.7	−15.7	15.6	8.3	14	11.2
	RCP85	2050s	18.6	25.5	76	98.6	102.8	80.3	33.1	19.7	37.7	15.1	15	12.1
		2090s	−7	11.9	143.4	188.3	91.3	14.2	−25.5	−32.4	−11.0	−17.2	−4.3	−10.6
MIROC5	RCP45	2050s	40.3	40.3	42.1	28.3	145.2	125.4	38.5	17.7	41.5	32.6	31.8	31.9
		2090s	43.7	43.8	58.4	44.5	91.6	75.6	1.4	−16.7	24.3	40.3	40.7	40.8
	RCP85	2050s	54.8	55.0	61.2	52.2	120.6	156.9	57.8	28.4	58.6	57.2	56.6	56.1
		2090s	45.4	47.3	85.6	99.4	254.6	79.8	−8.6	−21.6	18.0	45.3	44.4	43.3
MRI-CGCM3	RCP45	2050s	40.0	41.8	86.0	110.2	85.2	67.8	36.5	43.5	79.0	48.9	39.0	38.8
		2090s	45.7	52.6	95.7	120.9	78.0	77.6	35.1	29.1	61.0	54.2	49.6	48.5
	RCP85	2050s	60.8	63.5	121	140.9	92.3	104.9	64.1	49.1	89.3	67.1	61.1	58.0
		2090s	72.9	91.6	203.5	203.1	145.0	90.9	35.2	27.8	69.4	65.3	63.0	67.4
NorESM1-M	RCP45	2050s	10.6	19	80.4	104.6	151.4	64.2	27.3	19.2	43.3	19.6	14.7	14.9
		2090s	16	19.3	64.1	141	141	53.5	−5.3	−9.7	14.9	12.9	18.0	14.7
	RCP85	2050s	20.6	30.6	94.9	111.4	132.5	60.6	27.2	18.9	48.5	22.8	23.1	19.9
		2090s	9.3	16.9	110.3	104.1	103.9	29.7	−14.4	−16.4	0.5	0.5	8.0	6.8

-100 -50 0 50 100 %

Table-4. Monthly stream flow changes by CMIP5 climate as compared to contemporary flows by ERA-Interim, in %

We found that decline in the end-of-century average annual flow was (35% drop). While no significant differences were observed between river flow trend lines between the RCP 4.5 and RCP 8.5 scenarios, the latter has higher intra-annual variability and divergence over time.

In addition to the above-described seasonal low volumes, the timing of glacier runoff and snowmelt changes greatly thereby affecting the seasonality and inter-annual variability of river flow.

The decline of glaciers and snow storage upstream of the hydropower plant is quite evident (Figure-5). Our analysis shows the steepest glacier mass loss to occur at mid-century, around 2050–2070. The rate of glacier mass loss (Figure-6) can be directly translated to an additional discharge contribution. This comparison allows us to conclude that the rate of core mass loss yields about 5% additional high-flow seasonal discharge.

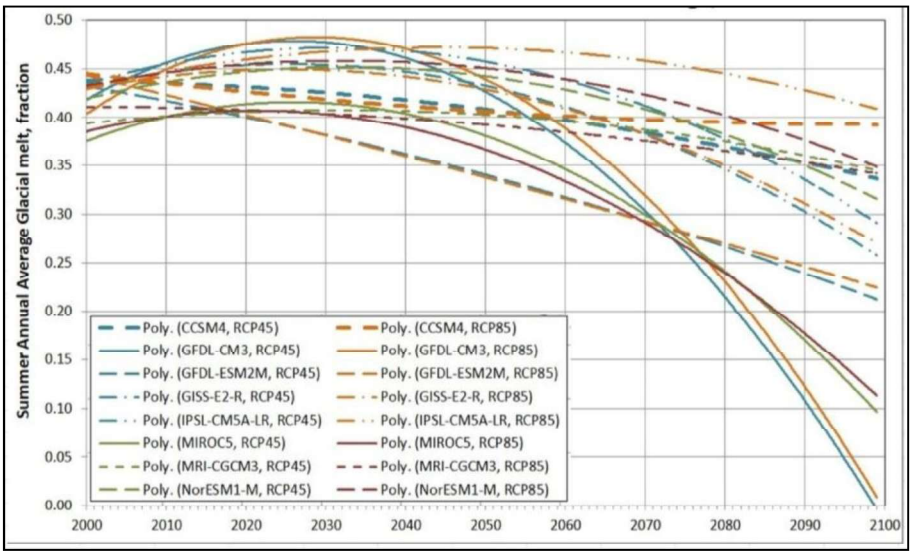


Figure-5: Summer Trend lines of Glacial Water Fractions in Discharge

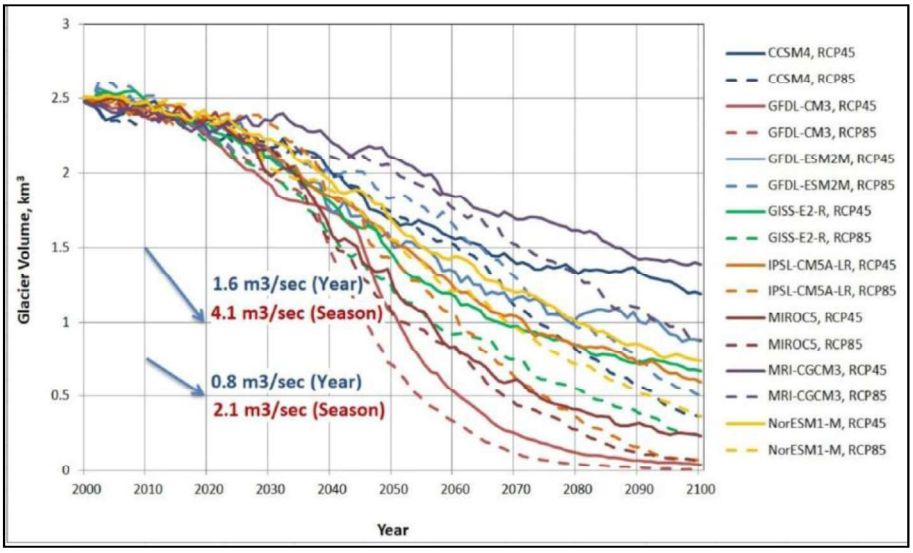


Figure-6: Glacier Volume in Naltar Catchment Area

In addition to the shifts in snow accumulation, melt seasons and glacier runoff evolution, changes in precipitation patterns and volumes will influence river flows over the 21st century. A moderate to strong decline in annual precipitation is projected toward the end of the century in most of the GCM/RCP combinations at Naltar. This directly impacts runoff and discharge volumes, along with the seasonality shifts due to changes in snow accumulation, melting seasons and the intensity of glacier runoff in the summer. Details of the inter-annual changes in discharge during the 21st century for study area illustrated in Figure-7.

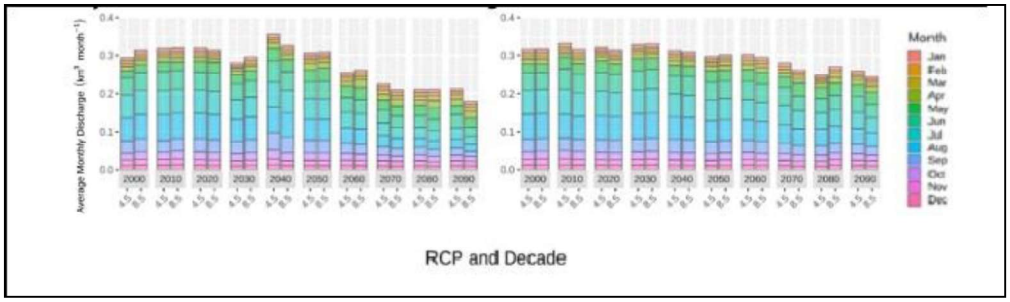


Figure-7: Decadal Discharge volume by month for two GCMs (GFDL-CM3 and NorESM1-M) and two RCPs (RCP 4.5 and RCP 8.5) from year 2000 to 2099.

Estimated changes in spring (March to June) river flow were found to be the largest compared to other seasons. Discharge at Naltar the estimated increase was almost an order of magnitude higher than observed flows (Tables 4 most GCMs with RCP 8.5). The source of water during the spring months was observed to be dominated by significantly higher volumes of snowmelt in RCP 8.5 as compared to RCP 4.5 (Figure-8). Summer (June to August) seasonal stream flow trends exhibited changes over the century (Figure-7). We observed an increase in flows from 15 to 19 $m^3 s^{-1}$ in 2060 and by the end of the century flow decreased to 4–18 $m^3 s^{-1}$. We also observed an increase in variability from 7 $m^3 s^{-1}$ in 2060 to 16 $m^3 s^{-1}$ by the end of the century corresponding to about 25 and 70% of the mean discharge. During the mid- summer months, lower river flow was seen in RCP 8.5 (Figure-7). From the standpoint of water availability for hydropower the most important flows are the hydrograph changes during the winter when stream flow values fall below plant capacity (see section “Hydroelectricity generation model results” below). Our study indicates a significant increase of winter flows from 2018 to 2100, specifically by 46.4% (Figure-8).

Figure-8. Average monthly snow and glacial melt fractions in discharge Solid line is for historical (2000–2017) and dashed line is for average combined future climates (2018–2100). Thick dashed line is all GCM/RCP combinations, top thin dashed line for all RCP 8.5 and bottom thin dashed line for RCP 4.5 scenarios. Where the sum of snow melt and glacier melt fractions is less than one, the remainder is composed of rainwater.

Source water analysis, which identifies the rain, glacier melt, and snow melt discharge fractions, is presented in Figure-8. Under all RCP scenarios, glacier

contributions decline significantly, with maximum contributions in July at 18–21%. Snowmelt contributes more to flow through most of the year; snow melt fractions are 50–58% from October through June historically, and decline to ~32% in the late summer months. This large contribution is due to the dominant presence of snowmelt in ground water storage, which returns to the surface flows through baseflow. This pattern continues in the future under both RCPs, though with a reduced amplitude. The maximum contribution is reduced to 40–52%, while the minimum contribution is increased to 40–45%. The glacier melt fraction shows a much shorter summer melt season with a greater maximum contribution (50%). Glacier melt contributions are projected to decrease during the summer melt season, declining from 50% to ~25% in July and August.

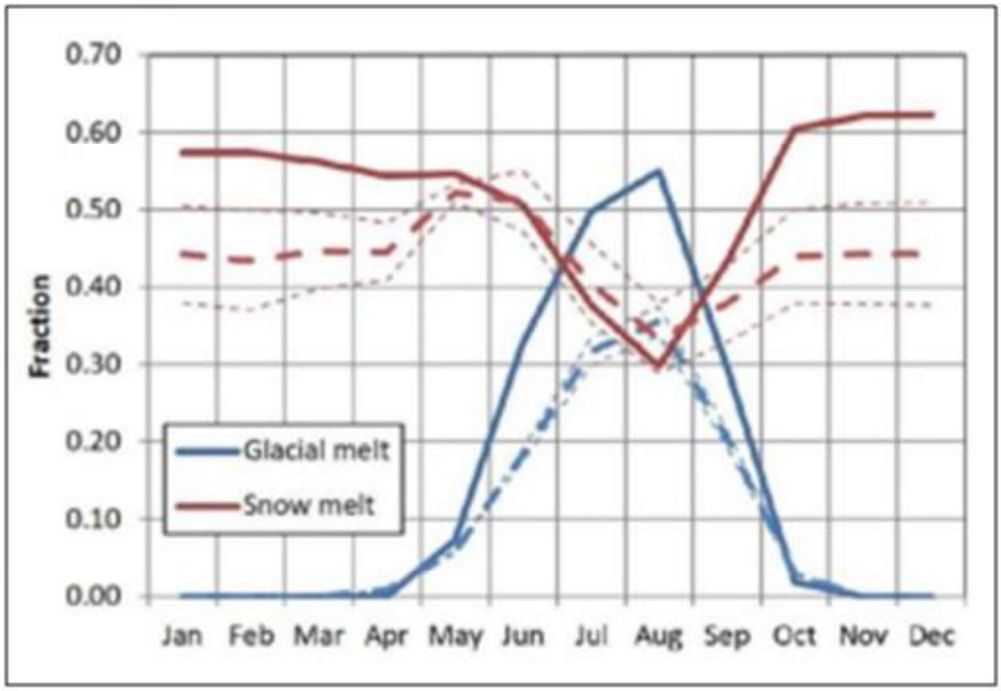


Figure-8

Comparison of contemporary and future component fractions indicate (a) an increase of glacier runoff at mid-century followed by sharp decline, (b) the snowmelt component declines in all simulations, and (c) there was an increase of total precipitation under some climate models (Figure-8). The recession of glaciers and snow storage in the catchment area above the study hydropower plant location is observed in Figure-5. Peak glacier melt (peak-water) occurs at mid 21st century, caused by accelerated glacier mass loss due to climate change, and is followed by a sharp decline as glacier volume becomes depleted (Figure-6). Snow melt, as a primary component of stream flow (Figure-9), also reflects the impact of climate change. Unlike glacier waters, the snow component does not have a peak and gradually declines toward the end of the century (Figure-8).

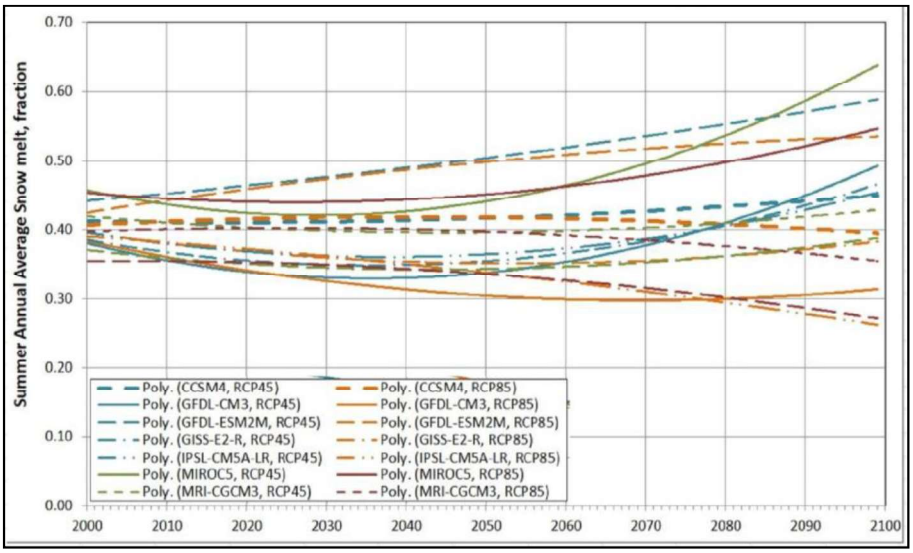


Figure-9: Summer Trend lines of Snowmelt Fraction in Discharge

Hydroelectricity Generation Model Results
Electricity Generation

We compared the observed monthly electricity generation levels with the HSM computed hydropower generation using the WBM stream flow rates for the 2000 through 2010 historical period. The HSM results were similar to historical average generation (Figure-10).

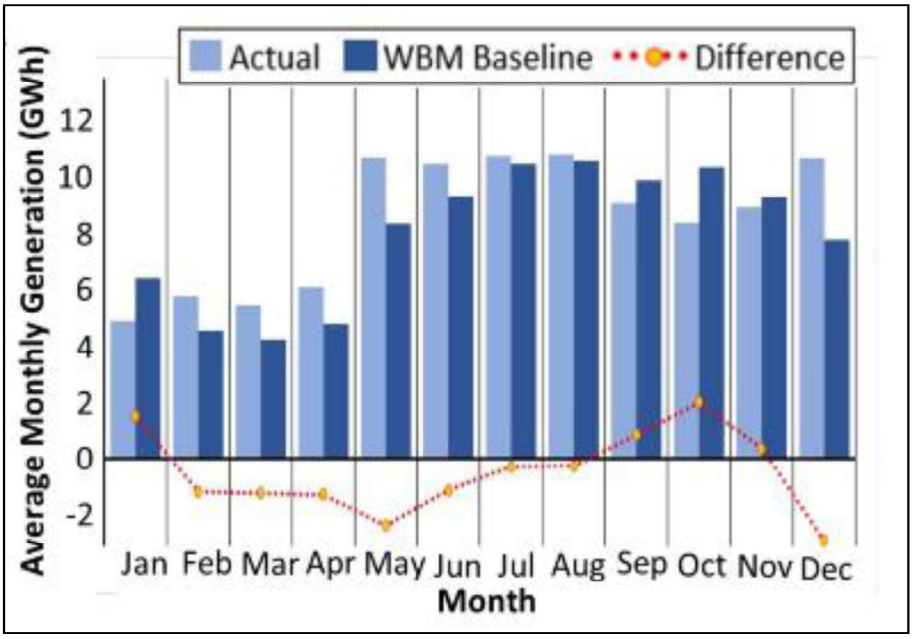


Figure-10: Comparison of historical average monthly generation and hydropower model simulation results

The modeled generation levels are noticeably lower than the historical average from February through June. During the summer high flow months, generation levels are largely unaffected by WBM underestimates, because during these periods water flow rates are above the maximum turbine rate a vast majority of the time (Figure-11).

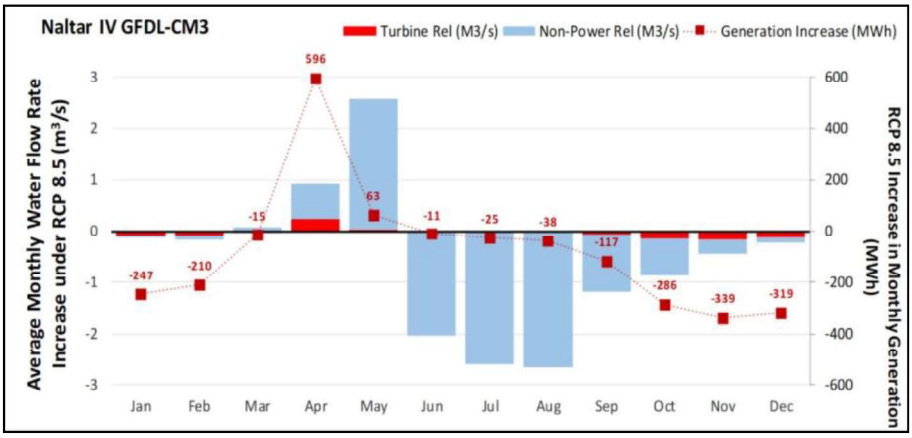


Figure-11: Average monthly increase in monthly hydropower production

Projection of Generation

Projections are based on (a) simulations that used WBM stream flow driven by all 16 GCM/RCP model combinations and (b) potential alternative hydropower plant development in the study basin. Figure-12 shows projected hydropower production, assuming that no changes will be made to Naltar and future hydropower resource development above the plant will be pure ROR resources. The estimated changes in annual electricity generation over the 80 years study period (trend lines) over all climate models range from a 7.5 increase to an 8.4% decrease (Figure-12 Left graph). The average change in generation over all climate models is expected to be less than 2 percent (Figure-12 Right graph). Annual variability in electricity generation was found to be about ± 25% is projected (Figure-13).

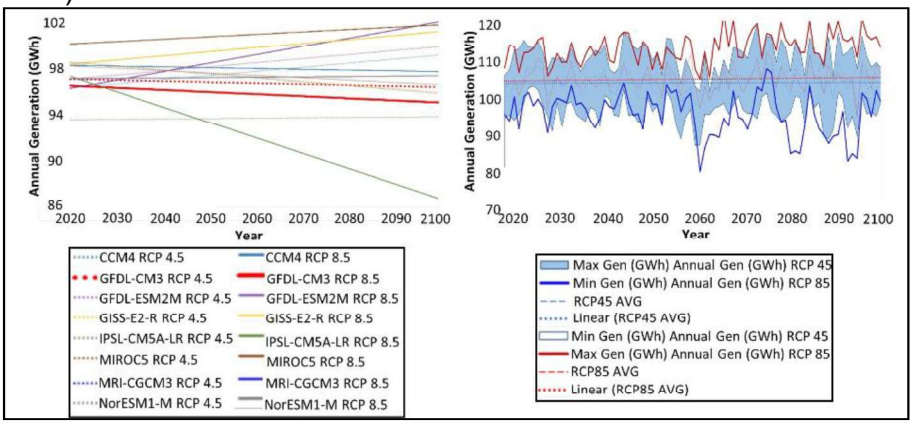


Figure-12: Trends and ranges of annual hydropower production

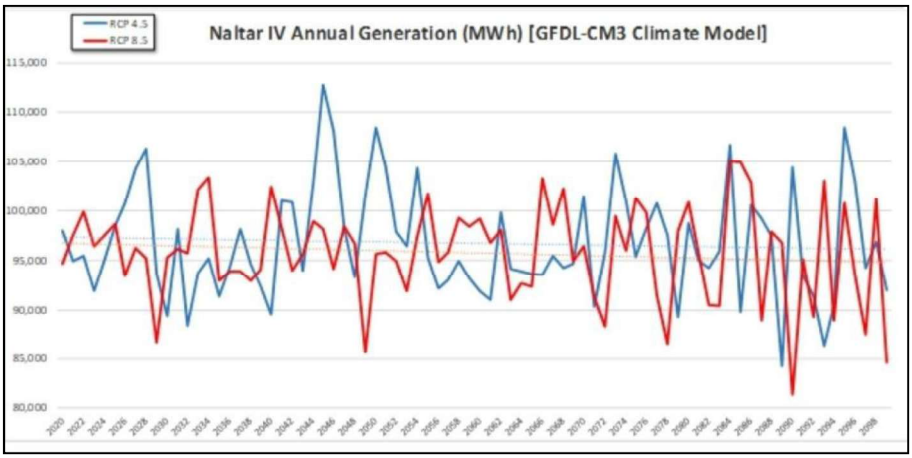


Figure-13: Annual hydropower production under RCP 4.5 and RCP 8.5 based on climate model

Changes in the timing of snow and glacier melt as well as precipitation dictate the impact of climate change on power production. Our results show that the projected increase in summertime river flow through mid-century does not impact hydropower generation. However, during lower flow periods, when power generation is below the capacity of the plant, the projected changes in inflows in various climate futures impact generation levels.

The difference between solid and dashed lines of the same color in Figure-12 indicates the difference in hydropower production between the RCP 4.5 and RCP 8.5 scenarios. The largest differences in generation between RCP 4.5 and RCP 8.5 scenarios were in February, March, April, October, November, and December. Although the gaps are relatively small, the differences were larger (Figures 14&15).

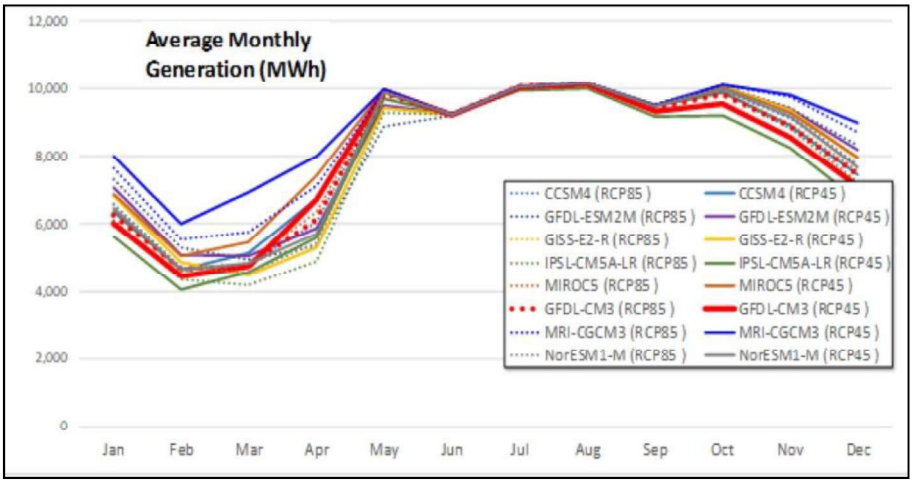


Figure-14: Average monthly hydropower production during the 80-year study period under RCP 4.5 and RCP 8.5 based on eight climate models for the static resource development future

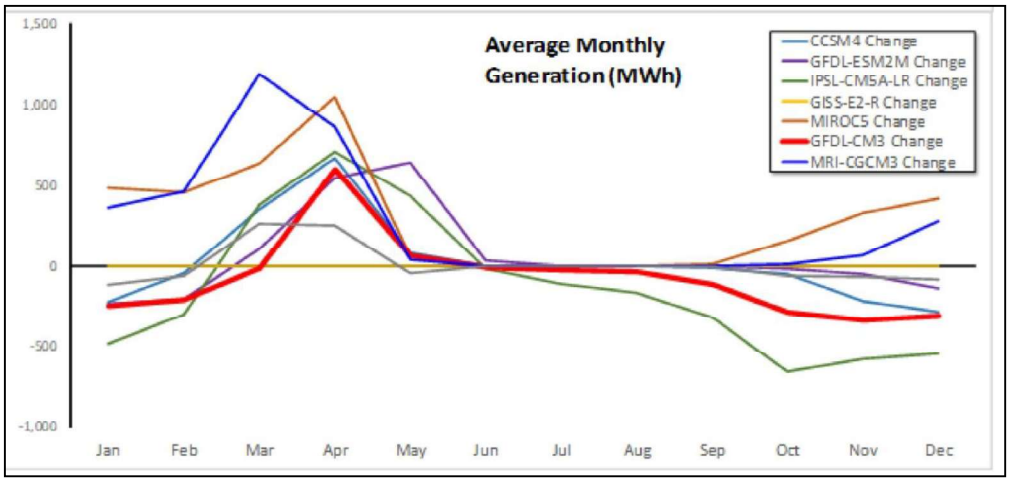


Figure-15: Impacts of a warmer climate on average monthly hydropower production

The characteristics of hydropower and associated upstream water storage have an impact on power production. Based on the current characteristics of Naltar the impacts are expected to be small, because the plant underutilize available water resources as measured by the large amounts of non- power water flows.

Under status quo operations in which water storage and hydropower resources do not change at Naltar, this high summertime inflow volatility does not impact power production because the lowest historical summertime flow rates far exceed the turbine flow rate maximums; that is power production is always at the physical maximum level. The impact of summertime inflow volatility on power system uncertainty is, therefore, inconsequential. In addition to inflow uncertainty, another uncertainty that impacts power production is the availability status of hydropower generating units. This uncertainty was modeled as random independent events during which time it was assumed that specific generating unit(s) were unavailable for power production. Figure-12 shows the band of future power system generation output and therefore one simple measure of uncertainty under both climate projections (RCP 4.5 and RCP 8.5).

Discussion

Interactions within and among physical processes and economic activities, such as those that occur during global climate change, are both complex and uncertain (Abbasi et al., 2017). Our study customized an integrated assessment-modeling framework to explore and learn about the relative impacts of projected changes in river flow and its constituent's snow and glacier melt and rainfall in Hunza basin. Because each individual tool in the framework is subject to modeling errors and uncertainty about the future, we used the framework to gain high-level insights into relative impact trends and magnitudes in the Hunza basin.

The WBM simulations of future river discharge showed reduced flows at Naltar. Separating the flow into the primary sources of rain, snow and glacier meltwater

shows decreased contribution of both glacier melt and snowmelt to river flow, with glacier meltwater reduced by 60%. A strong seasonal shift in river flow is consistent across most GCMs and RCPs. There is a significantly higher variability across the models toward the end of the century, which is expected given the uncertainties in running these GCMs so far into the future. An earlier spring melt and later accumulation of the snowpack reduce the length of the winter low-flow period, and this is more pronounced. We also observed a reduced summer river flow in the model output, although the time of year is different due to lower contributions of glacier meltwater at Naltar the lower summer flows are mostly concentrated in July and August. Lutz (2016) found projected river flow in the Hunza decreased during the melt season under both RCP 4.5 and RCP 8.5. The fall and spring shifts in melt move more of the snowmelt away from the summer period, causing overall reduced river flows during this high-flow period. Tahir et al. (2015) found that despite stable or increasing snow cover trends, the river flow trend is decreasing in Hunza.

The results from our glacier and hydrology modeling components, showing increasing glacier melt driving increasing river discharge from glaciers and a subsequent decline in river flow, are a characteristic of “peak water” (Kraaijenbrink et al., 2017; Huss and Hock, 2018). These changes are strongest in the RCP 8.5 simulations. Immerzeel and Bierkens (2012) found the dominant factors for changing water supply in the Indus and Ganges basins to be uncertainty in precipitation, population growth, and in the Indus only, ground water depletion. Lutz et al. (2014) focused on the upstream basins in HMA and showed the greatest future contribution to runoff was glacier melt in the Indus and rainfall in the Ganges. In both cases the metrics were based on large areas where the results used basin wide (Immerzeel and Bierkens, 2012) and aggregated HMA headwaters (Lutz et al., 2014) that do not necessarily indicate the dominant factors at play in the small, headwater basins explored in this research.

The impact of changes in annual inflows does not translate to significant changes in annual power production at Naltar-IV hydropower power plant. However, the timing of water inflows during the year and projected changes in flow during low-flow periods in a changed climate is important. In both RCP 4.5 and RCP 8.5 scenarios, during most of the year most of the river water bypasses the Naltar hydropower plants because river flow rates exceed the maximum rate of turbine-water-flow. Power plant therefore mostly operate at the maximum physical limit and are unresponsive to climate change under the current system configuration. However, with an upcoming large storage type hydropower four km upstream from the power plant may influence the power plant especially in drier months. While GCM/RCP results agree that changes are expected to be small at Naltar. A sub-basin-level analysis for the whole region will help the government and the private sector make informed decisions and assess financial risks based on site-specific analyses that encompass the power grid and hydrological dynamics, using an ensemble of projected flows driven by a set of projected downscaled climatic variables.

Summary of the Results

- Summer discharge initially tends to increase by about 10% at the mid-century, and then experience a sharper decline by about 50% toward the end of the 21st century
- Significant increase of winter flows from 2018 to 2100, specifically by 46.4%
- Glacier contributions decline significantly, with maximum contributions in July at 18–21%.
- Snowmelt contributes more to flow through most of the year; snow melt fractions are 50–58% from October through June historically, and decline to ~32% in the late summer months
- Glacier melt fraction shows a much shorter summer melt season with a greater maximum contribution (50%)
- Glacier melt contributions are projected to decrease during the summer melt season, declining from 50% to ~25% in July and August
- Estimated changes in annual electricity generation over the 80 years study period over all climate models range from a 7.5% increase to an 8.4% decrease
- Average change in generation over all climate models is expected to be less than 2%
- Annual variability in electricity generation was found to be about ± 25% is projected
- Projected increase in summertime river flow through mid-century does not impact hydropower generation
- However, during lower flow periods, when power generation is below the capacity of the plant, the projected changes in inflows in various climate futures impact generation levels
- The largest differences in generation between RCP 4.5 and RCP 8.5 scenarios were in February, March, April, October, November, and December

Table-5: Existing Hydro Power Projects in Operation in Snow & Glacier Fed Region of Pakistan				
Sr. No.	**Name of HydroPower**	**Location**	**Province**	**Installed Capacity MW**
1	Naltar	Gilgit	Gilgit-Baltistan	18.00
2	Gilgit	Gilgit	Gilgit-Baltistan	10.63
3	Skardu-I	Skardu	Gilgit-Baltistan	6.96
4	Chilas-I	Chilas	Gilgit-Baltistan	5.62
5	Hunza	Hunza	Gilgit-Baltistan	5.13
6	Shyok	Shyok	Gilgit-Baltistan	4.85
7	Astore	Astore	Gilgit-Baltistan	3.11
8	Kachura Ph-II	Skardu	Gilgit-Baltistan	3.00
9	Ghizar	Ghizar	Gilgit-Baltistan	2.00
10	Thak	Chilas	Gilgit-Baltistan	2.00
11	Phandar	Ghizar	Gilgit-Baltistan	2.00
12	Bordas	Ghanche	Gilgit-Baltistan	2.00
13	84 Small Hydel Power Projects less than 2MW	Various Locations	Gilgit-Baltistan	47.70
Total				**113.00**

References

Abbasi, S. S., Ahmad, B., Ali, M., Anwar, M. Z., Dahri, Z. H., Habib, N., et al. (2017). The Indus Basin: A Glacier-Fed Lifeline for Pakistan. Kathmandu: HI-AWARE.

Ahmed, M., and Suphachalasai, S. (2014). Assessing the Costs of Climate Change and Adaptation in South Asia. Available at: http://www.adb.org/sites/default/files/pub/2014/assessing- costs- climate- change- and- adaptation- south- asia.pdf (accessed February 23, 2015).

Alford, D., and Armstrong, R. (2010). The role of glaciers in stream flow from the Nepal Himalaya. Cryosphere Discuss. 4, 469–494. doi: 10.5194/tcd-4-469-2010

Bajracharya, S., Maharjan, S., Shrestha, F., Bajracharya, O., and Baidya, S. (2014). Glacier Status in Nepal and Decadal Change from 1980 to 2010 Based on Landsat Data. Geneva: World Meteorological Organization.

Bajracharya, S. R., and Shrestha, B. (eds) (2011). The Status of Glaciers in the Hindu Kush-Himalayan Region. Kathmandu: ICIMOD.

Bashir, F., Zeng, X., Gupta, H., and Hazenberg, P. (2017). A hydrometeorological perspective on the karakoram anomaly using unique valley-based synoptic weather observations. Geophys. Res. Lett. 44, 470–410. doi: 10.1002/2017GL075284

Brun, F., Berthier, E., Wagnon, P., Kääb, A., and Treichler, D. (2017). A spatially resolved estimate of high mountain asia glacier mass balances from 2000 to 2016. Nat. Geosci. 10, 668–673. doi: 10.1038/ngeo 2999

Federer, C. A., Vörösmarty, C., and Fekete, B. (1996). Intercomparison of methods for calculating potential evaporation in regional and global water balance models. Water Resour. Res. 32, 2315–2321. doi: 10.1029/96wr00801

Fekete, B. M., Vorosmarty, C. J., Roads, J. O., and Willmott, C. J. (2004). Uncertainties in precipitation and their impacts on runoff estimates. J. Clim. 17, 294–304. doi: 10.1175/1520- 0442(2004)017< 0294:uipati> 2.0.co;2

Forsythe, N., Fowler, H. J., Li, X. F., Blenkinsop, S., and Pritchard, D. (2017). Karakoram temperature and glacial melt driven by regional atmospheric circulation variability. Nat. Clim. Chang. 7, 664–670. doi: 10.1038/NCLIMATE3361

Fowler, H. J., and Archer, D. R. (2006). Conflicting signals of climate change in the Upper Indus basin. J. Clim. 19, 4276–4293. doi: 10.1175/jcli3860.1

Hamon, W. R. (1961). Estimating potential evapotranspiration. J. Hydra. Div. 87, 107–120.

Huss, M., and Hock, R. (2015). A new model for global glacier change and sea-level rise. Front. Earth Sci. 3:54. doi: 10.3389/feart.2015.00054

HydroSHEDS, (2019). USGS Hydrosheds. Reston, VA: USGS.

Immerzeel, W., and Bierkens, M. (2012). Asia's water balance. Nat. Geosci. 5, 841–842. doi: 10.1038/ngeo1643

Immerzeel, W. W., Droogers, P., de Jong, S. M., and Bierkens, M. F. P. (2009). Large-scale monitoring of snow cover and runoff simulation in Himalayan river basins using remote sensing. Remote Sens. Environ. 113, 40–49. doi: 10.1016/j.rse.2008.08.010

Kapnick, S. B., Delworth, T. L., Ashfaq, M., and Malyshev, S. (2014). Snowfall less sensitive to warming in Karakoram than in Himalayas due to a unique seasonal cycle. Nat. Geosci. 7, 834–840. doi: 10.1038/ngeo2269

Kessides, I. N. (2013). Chaos in power: pakistan's electricity crisis. Energy Policy 55, 271–285. doi: 10.1016/j.enpol.2012.12.005

Khokhar, S., Min, X., and Chu, Q. (2015). Electricity crisis and energy efficiency to poultry production in Pakistan. World Poult. Sci. J. 71, 539–546. doi: 10.1017/S0043933915002123

Kraaijenbrink, P., Bierkens, M., Lutz, A., and Immerzeel, W. W. (2017). Impact of a global temperature rise of 1.5 degrees Celsius on Asia's glaciers. Nature 549, 257–260. doi: 10.1038/nature23878

Lammers, R. B., Shiklomanov, A. I., Vorosmarty, C. J., Fekete, B. M., and Peterson, B. J. (2001). Assessment of contemporary arctic river runoff based on observational discharge records. J. Geophys. Res. 106, 3321–3334. doi: 10.1029/2000jd900444

Lehner, B., and Grill, G. (2013). Global river hydrography and network routing: baseline data and new approaches to study the world's large river systems. Hydrol. Process. 27, 2171–2186. doi: 10.1002/hyp.9740

Liu, J., Hertel, T. W., Lammers, R. B., Prusevich, A., Baldos, U. L. C., Grogan, D. S., et al. (2017). Achieving sustainable irrigation water withdrawals: global impacts on food security and land use. Environ. Res. Lett. 12:104009. doi:10.1088/1748-9326/aa88db

Lutz, A. F. (2016). Impact of Climate Change on the Hydrology of High Mountain Asia. Ph.D. thesis, Universiteit Utrecht, Utrecht.

Ministry of Finance, (2013). Pakistan Economic Servey 2012-2013 Chapter-14 Energy, 187–188. New Delhi: Ministry of Finance.

Mishra, S. K., Hayse, J., Veselka, T., Yan, E., Kayastha, R. B., LaGory, K., et al. (2018). An integrated assessment approach for estimating the economic impacts of climate change on River systems: an application to hydropower and fisheries in a Himalayan River, Trishuli. Environ. Sci. Policy 87, 102–111. doi: 10.1016/j.envsci.2018.05.006

Pradhananga, N. S., Kayastha, R. B., Bhattarai, B. C., Adhikari, T. R., Pradhan, S. C., Devkota, L. P., et al. (2014). Estimation of discharge from Langtang River basin, Rasuwa, Nepal, using a glacio-hydrological model. Ann. Glaciol. 55, 223–230. doi: 10.3189/2014AoG66A123

Rehman, A. S., Cai, Y., Hussain, N., and Das, G. (2019). Energy-environment-economy nexus in pakistan : lessons from a PAK-TIMES Model. Energy Policy 126, 200–211. doi: 10.1016/j.enpol.2018.10.031

Rennick, M. A. (1977). Parameterization of tropospheric lapse rates in terms of surface-temperature. J. Atmos. Sci. 34, 854–862. doi: 10.1175/1520- 0469(1977) 034< 0854:tpotlr> 2.0.co;2

RGI Consortium, (2017). Randolph Glacier Inventory – A Dataset of Global Glacier Outlines: Version 6.0. Technical Report, Global Land Ice Measurements from Space. Colorado: Digital Media.

Rounce, D., Hock, R., Shean, D., and Khurana, T. (2020). Quantifying glacier mass change in High Mountain Asia through 2100 using the open-source python glacier evolution model (PyGEM). Front. Earth Sci. 7:331. doi: 10.3389/feart. 2019.00331

Shean, D., Montesano, P., Rounce, D., Bhushan, S., Arendt, A., and Osmanoglu, B. (2020). A systematic, regional assessment of High-mountain Asia mass balance. Front. Earth Sci. 7:363. doi: 10.3389/feart.2019.00363

Smith, T., and Bookhagen, B. (2018). Changes in seasonal snow water equivalent distribution in high mountain Asia (1987 to 2009). Sci. Adv. 4:e1701550. doi: 10.1126/sciadv.1701550

Tachikawa, T., Kaku, M., Iwasaki, A., Gesch, D. B., Oimoen, M. J., Zhang, Z., et al. (2011). "ASTER global digital elevation model version 2 - summary of validation results," in Paper Presentation at the 39th ASTER Science Team Meeting, Tokyo.

Tahir, A. A., Chevallier, P., Arnaud, Y., Ashraf, M., and Bhatti, M. T. (2015). Snow cover trend and hydrological characteristics of the Astore River basin (Western Himalayas) and its comparison to the Hunza basin (Karakoram region). Sci. Total Environ. 505, 748–761. doi: 10.1016/j.scitotenv.2014.10.065

Tahir, A. A., Chevallier, P., Arnaud, Y., Neppel, L., and Ahmad, B. (2011). Modeling snowmelt-runoff under climate scenarios in the Hunza River basin, Karakoram Range, Northern Pakistan. J. Hydrol. 409, 104–117. doi: 10.1016/j.jhydrol.2011. 08.035

Vörösmarty, C. J., Green, P., Salisbury, J., and Lammers, R. B. (2000). Global water resources: vulnerability from climate change and population growth. Science 289, 284–288. doi: 10.1126/science.289.5477.284

Water and Power development authority Report [WAPDA], (2013). Unpublished Report Pakistan Water and Power Development Authority. Lahore: WAPDA.

Wisser, D., Fekete, B. M., Vorosmarty, C. J., and Schumann, A. H. (2010). Reconstructing 20th century global hydrography: a contribution to the Global Terrestrial Network- Hydrology (GTN-H). Hydrol. Earth Syst. Sci. 14, 1–24. doi: 10.5194/hess- 14- 1- 2010